

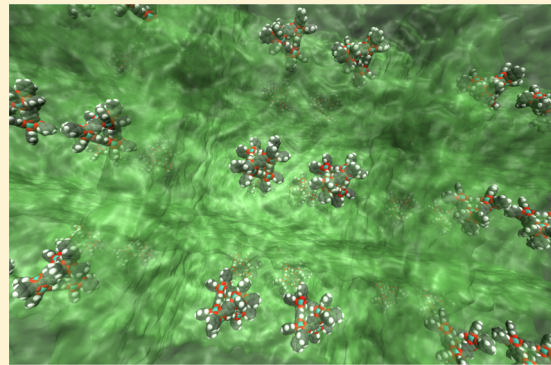
# A Combined Experimental and Computational Study on the Stability of Nanofluids Containing Metal Organic Frameworks

Harsha V. R. Annareddy,<sup>†</sup> Satish K. Nune,<sup>‡</sup> Radha Kishan Motkuri,<sup>‡</sup> B. Peter McGrail,<sup>‡</sup> and Liem X. Dang\*,<sup>†</sup>

<sup>†</sup>Fundamental and Computational Sciences Directorate and <sup>‡</sup>Energy and Environment Directorate, Pacific Northwest National Laboratory, Richland, Washington 99352, United States

## Supporting Information

**ABSTRACT:** Computational studies on nanofluids composed of metal organic frameworks were performed using molecular modeling techniques. Grand Canonical Monte Carlo simulations were used to study the adsorption behavior of 1,1,1,3,3-pentafluoropropane (R-245fa) in a MIL-101 metal organic frameworks at various temperatures. To understand the stability of the nanofluid composed of MIL-101 particles, we performed molecular dynamics simulations to compute potentials of mean force between hypothetical MIL-101 fragments terminated with two different kinds of modulators in R-245fa and water. Our computed potentials of mean force results indicate that the metal organic frameworks particles tend to disperse better in water than in R-245fa. The reasons for this difference in dispersion were analyzed and are discussed in the paper. Our results agree with experimental results indicating that the potential models employed and modeling approaches provide good descriptions of molecular interactions and the reliabilities.



## I. INTRODUCTION

Nanofluids are gaining considerable attention because of their potential application in power generation from renewable energy sources such as geothermal, solar, industrial waste heat, and biomass combustion.<sup>1</sup> Nanofluids are liquids containing low concentrations of nanometer-sized particles. The term “nanofluids” was coined by researchers at Argonne National Laboratory to describe the suspension of nanoparticles in base fluids such as water, ethylene glycols, oils, etc.<sup>2</sup> Conventional fluids have poor thermal conductivity compared to solids; the thermal conductivity can be enhanced by dispersing the solid particles in fluids. This fundamental concept has been a topic of interest for a long time.<sup>3</sup> Early studies were confined only to millimeter or micrometer-sized particles. The stability of the suspension is the major challenge of this approach, as the large particles tend to settle rapidly. The use of nanoparticles shows promise as a solution to this problem.<sup>4</sup> Because of their smaller size, nanoparticles remain suspended in fluids for longer times, and they also provide a larger surface area per unit volume, which is important for improving heat transfer characteristics. Commonly investigated nanoparticles include oxides ( $\text{Al}_2\text{O}_3$ ,  $\text{CuO}$ ), metal carbides ( $\text{SiC}$ ), metals ( $\text{Al}$ ,  $\text{Cu}$ ), and carbon nanotubes. Drawbacks associated with metal and oxide nanoparticles include mismatches in the densities of the particles and the working fluid, mass and volume displacement of working fluids, and the need for surfactant stabilizers that also cause additional complications such as changes in boiling point, zeotropic behavior, increased viscosity, etc.

McGrail and co-workers have introduced a new class of nanofluids called metal organic heat carriers (MOHCs).<sup>5,6</sup> These new nanofluids contain nanoparticles made of metal organic frameworks (MOFs), which are porous crystalline materials that are formed by molecular assemblies constructed by coordination bonds between metal ion clusters and organic molecules known as linkers. MOFs have been studied extensively for various applications.<sup>7–16</sup> In addition to their large surface area, permanent porosity, structure varieties, and stability, MOFs offer an opportunity to engineer efficient nanofluids at a molecular level through various combinations of metals and linkers to improve their performance in thermal vapor–liquid compression cycles.

However, the stability of the MOF particle dispersion in base working fluids is key for successful application of MOHCs in heating and cooling devices. Introduction of surfactants into working fluids is a common technique used to stabilize nanofluid suspensions. However, this approach has various drawbacks including changes in boiling point, zeotropic behavior, increased viscosity, reduced heat transfer coefficients, and many other changes in physical properties that often degrade the performance of nanofluids. Our current research

**Special Issue:** Branka M. Ladanyi Festschrift

**Received:** August 6, 2014

**Revised:** December 5, 2014

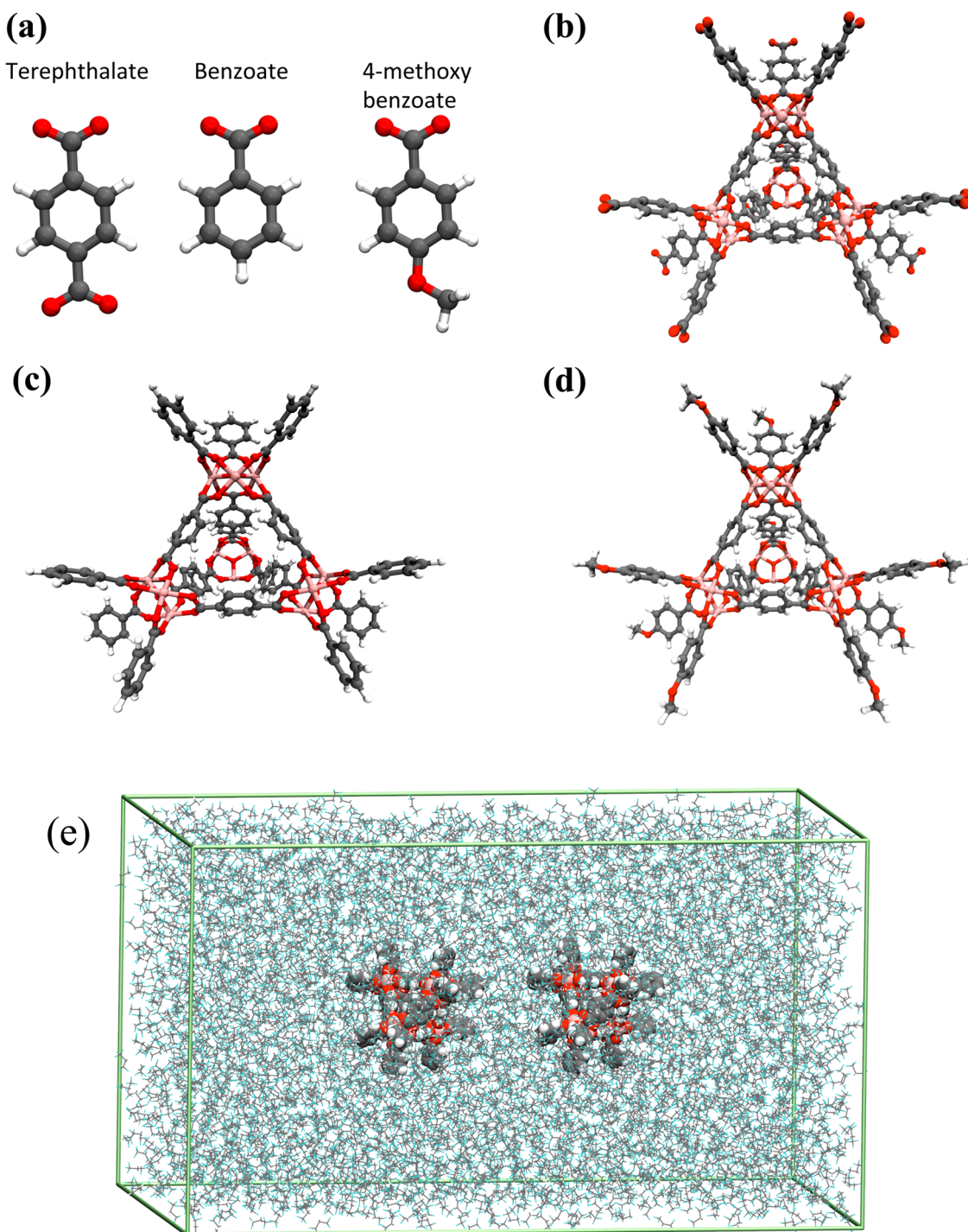


**Figure 1.** (a) Linker and modulator units. (b) Fragment of MIL-101. (c) Fragment of MIL-101 terminated with benzoate modulator. (d) Fragment of MIL-101 terminated with 4-methoxybenzoate modulator. (e) A representative simulation box used for PMF calculations (two MIL-101 fragments in R-245fa solvent).

efforts focus on chemical functionalization of the nanoparticle surface to attain stable nanofluid suspensions. A molecular-level understanding of the nanoparticle solvation process and factors influencing dispersion stability is necessary to develop stable and better-performing nanofluids. Computational techniques such as molecular dynamics (MD) simulations can provide more molecular-level insight into the interfacial behavior of a base fluid with the MOF surface. We used a solution analogy that describes the immersed MOF as a large, spatially suspended, and infinitely dilute nanoparticle.

In this article, we focused on nanofluids containing MIL-101 (MIL is the abbreviation of Materials of Institute Lavoisier) MOF particles. MIL-101, a chromium terephthalate-based MOF, is a framework formed through the connection of supertetrahedra by corner sharing. The supertetrahedra structure is made of  $\text{Cr}_3\text{O}$  units at four vertices, which are linked through six terephthalate (1,4-benzenedicarboxylate) linkers forming the edges of tetrahedron. MIL-101 was specifically chosen because of its high porosity and high water or gas uptake. We studied dispersion stabilities in water and in

1,1,1,3,3-pentafluoropropane (R-245fa), which is a hydrofluorocarbon with a broad range of applications as a blowing agent, solvent, aerosol, and working fluid. The primary attribute of R-245fa is that it has no ozone depletion potential and minimal toxicity. Its physical properties and environmental characteristics make it more suitable for various heat transfer applications. The size of MOF nanoparticles is controlled using modulators with molecular structures that are similar to the linkers, but with only one carboxylate group. Two kinds of modulators (benzoate and 4-methoxybenzoate) are shown in Figure 1a. It can be seen in the figure that the two molecules contain only one carboxylate group. Once these modulators are bound to the metal complex, the extension of the framework will be terminated because no carboxylate group is present on the other end. Modulators with different functionalization also can be used for the surface modification of the nanoparticle.

First, we studied the structure and dynamics of pure liquid R-245fa and then its adsorption behavior and temperature dependence in MIL-101. To gain molecular-level insight on preferential adsorption sites in MIL-101, we performed MD simulations and calculated radial distribution functions (RDFs). We employed the potentials of mean force (PMF) approach to evaluate the interaction between MOF nanoparticles dispersed in water and R-245fa. The rest of this article is organized as follows. In Section II, the details of methods and simulations are reported. Results and discussion are presented in Section III, and the conclusions are discussed in Section IV.

## II. METHODS AND SIMULATION

All MD simulations in this study were performed using a modified version of the Amber 9 package.<sup>17</sup> Grand Canonical Monte Carlo (GCMC) simulations were performed using the Music program.<sup>18</sup> The force field parameters for R-245fa were taken from the literature. Charges for this molecule were computed through ab initio RESP-fit at the Hartree–Fock/6-311+G\* theory level using the Gaussian 98 program.<sup>19</sup> All intramolecular bond parameters and the original Lennard-Jones (LJ) parameters were taken from GAFF.<sup>20,21</sup> The LJ parameters were slightly adjusted to match the experimental enthalpy of vaporization and liquid densities. To obtain the appropriate parameters for R-245fa, several MD simulations were run using a simulation box of 500 molecules in an NPT ensemble at 273 K and 1 bar. The potential parameters for R-245fa are provided in the Supporting Information.

The GCMC simulation box consisted of one unit cell of MIL-101. Force field parameters for MIL-101 were obtained from the density-functional theory studies of Chen et al.<sup>22</sup> The periodic boundary conditions were employed in three dimensions. Intermolecular interactions between the MOF framework and host molecules were described by LJ and electrostatic interactions. The SPC/E water model was used to describe the water–water interactions.<sup>23</sup> The interactions between MOF, R-245fa, and water were modeled using simple combining rules.<sup>24</sup> A spherical cutoff radius of 20 Å is used for both LJ and electrostatic interactions with the use of damped shifted method developed by Wolf et al. for electrostatic interactions.<sup>25</sup> In a GCMC simulation, chemical potential ( $\mu$ ), volume ( $V$ ), and temperature ( $T$ ) were kept constant, and the number of particles was allowed to change. All the simulation runs were carried out with four types of moves: (1) molecular displacement, (2) molecular rotation, (3) insertion of a molecule with random orientation into a random position in the system, and (4) deletion of a randomly chosen molecule

from the system. At each pressure point, we performed  $1 \times 10^7$  trial moves for GCMC simulations.

In this work, we studied the effects of two different kinds of modulators: benzoate and 4-methoxybenzoate as illustrated in Figure 1a. To compute the PMF, we took a portion of rigid nanoparticle from the MIL-101 framework as shown in Figure 1b. We then replaced the terminal terephthalate units with modulator units. The MOF fragments after substitution with the modulators are shown in Figures 1c and 1d, and they were solvated in water and R-245fa. The simulation boxes consisted of 27 004 solvent molecules for the water system and 4522 solvent molecules for the R-245fa system. We determined the number of solvent molecules by using the aqueous solution density that corresponds to the pure liquid density (i.e., 1 g/cm<sup>3</sup> for water solvent). In addition, the number ‘27 004 solvent molecules’ was chosen so box lengths would be large enough to minimize image effects when separation distances between nanoparticles are large. The representative simulation box of MOF fragments in R-245fa is shown in Figure 1e also.

We computed the PMF using a constrained MD technique. Using this approach, we evaluated the free-energy profiles as a function of the center-of-mass separation between the two MOF fragments. Equation 1 is used to compute the mean force along the reaction coordinate for various solvent configurations.

$$F(r) = \frac{1}{2} \langle \hat{r}_{\text{com}} \cdot (\vec{F}_A - \vec{F}_B) \rangle \quad (1)$$

Here,  $\vec{F}_A$  and  $\vec{F}_B$  are the forces acting on fragments A and B, respectively. The term  $\hat{r}_{\text{com}}$  is the unit vector along AB, given eq 2, and  $\langle \dots \rangle$  represents the average over several configurations.

$$\hat{r}_{\text{com}} = \frac{\vec{r}_{AB}}{|\vec{r}_A - \vec{r}_B|} \quad (2)$$

We carried out a series of MD simulations at various center of mass separation distances with increments of 0.5 Å. In each of these MD simulations, the center of mass separation between the two MOF fragments was fixed, and the solvent configurations were sampled to evaluate the mean force ( $F(r)$ ) using eq 1. At each distance,  $F(r)$  was obtained through an average over 5 ns of simulation. The PMFs were computed using these  $F(r)$  values and eq 3.

$$W(r) = - \int_{r_0}^r \langle F(r) \rangle dr \quad (3)$$

All these simulations are performed in an NVT ensemble using the periodic boundary conditions on all three directions with a time step of 2 fs. PMFs were computed in water and R-245fa. We used the Ewald summation technique to handle long-range electrostatic interactions and the SHAKE algorithm to constrain the internal geometries of water and R-245fa.<sup>26,27</sup>

The gas sorption experiments were carried out using an Intelligent Gravimetric Analyzer (IGA) from Hiden Instruments. The methanol exchanged bulk MIL-101 was activated at 250 °C with a heating rate of 5 °C/min for 12 h under vacuum. After activation, the dry mass of the adsorbent was corrected, and the experimental temperatures were maintained throughout each sorption experiment using a water bath. A specific amount of R-245fa fluorocarbon introduced into the sample chamber while monitoring the weight gain and the pressure was maintained at each set point for about 20 min until equilibrium was established. The mass uptake was measured as a function of pressure until equilibrium was established, at which point the

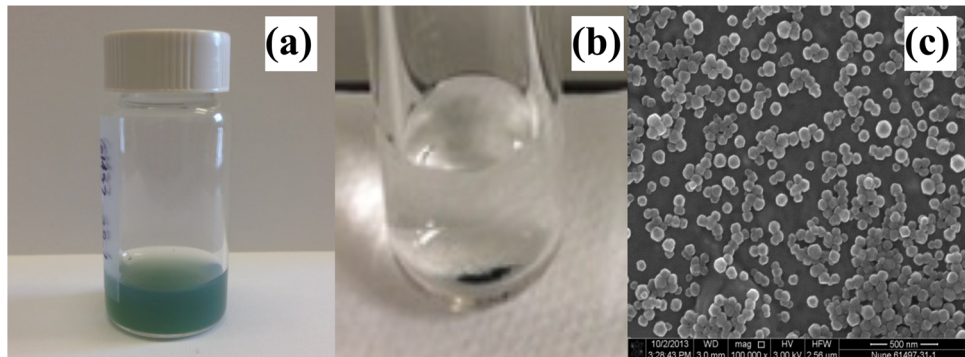


**Figure 2.** Illustrations of dispersed nano-MIL-101 (4-methoxy terephthalic acid modulator) in (a) water and (b) R-245fa. (c) SEM image of nano-MIL-101.

pressure was increased to the next set pressure value and the subsequent uptake was measured until equilibrium was re-established. Similarly, the sorption experiments were measured at four different temperatures: 283, 298, 313, and 333 K. The experimentally measured R-245fa loadings in MIL-101 were fitted with the dual-site Langmuir–Freundlich model, and the fits obtained are excellent over the entire range of pressures at all temperatures. The interaction strength between R-245fa and MIL-101 was calculated using the isosteric heats of adsorption ( $q_{st}$ ), which is determined from the adsorption isotherms at different temperatures using the Clasius–Clapeyron equation. The value of  $q_{st}$  for R-245fa in MIL-101 at a constant loading was found to be  $\sim 8.2$  kcal/mol, which indicates gas interaction with the relatively homogeneous pore system.

In addition, the experimental nanofluids used in this study were prepared according to the following procedure. To a fresh vial of  $\text{Cr}(\text{NO}_3)_3 \cdot 9\text{H}_2\text{O}$  (330 mg, 0.82 mmol), terephthalic acid (136.9 mg, 0.82 mmol), modulator (4-methoxy benzoic acid; 5.1 mg, 0.033 mmol), and water (25 mL) were added. The resulting heterogeneous solution/suspension was mixed thoroughly and sonicated for 5 min at room temperature followed by heating at 180 °C for 4 h in a Teflon-lined autoclave. The reaction mixture was allowed to cool to room temperature and filtered with a 0.2-μm centrifuge filter to remove the unreacted/recrystallized terephthalic acid. Further high-speed centrifugation of the resulting colloidal suspension left a wet green pellet, which was washed with water three times and then with methanol two times to obtain a pale green, pure nano-MIL-101 powder. A similar procedure was used for other modulator including benzoic acid. Dispersion of wet green nano-MIL-101 pellet in water and then sonicated for 10 min yielded stable aqueous colloidal suspensions (up to 1 wt %; Figure 2a). On the other hand, green dry powders of nano-MIL-101 did not disperse in R-245fa at all (Figure 2b). The SEM image shown in Figure 2c shows the homogeneous distribution of near spherical particles. To understand this behavior at the molecular level, we performed detailed MD simulations on these systems.

### III. RESULTS AND DISCUSSION

**A. Pure R-245fa.** We begin this section with the discussion of pure liquid R-245fa, which has a boiling point of 15 °C. The average density obtained through the NPT simulation is 1.40 g/cm<sup>3</sup> at 0 °C, which is in good agreement with the experimental density ( $\sim 1.404$  g/cm<sup>3</sup>). In Figure 3a, we show the RDF for the central carbon atoms of R-245fa. The RDF plot clearly shows two solvation shells. The first and second peaks are at 5.65 and

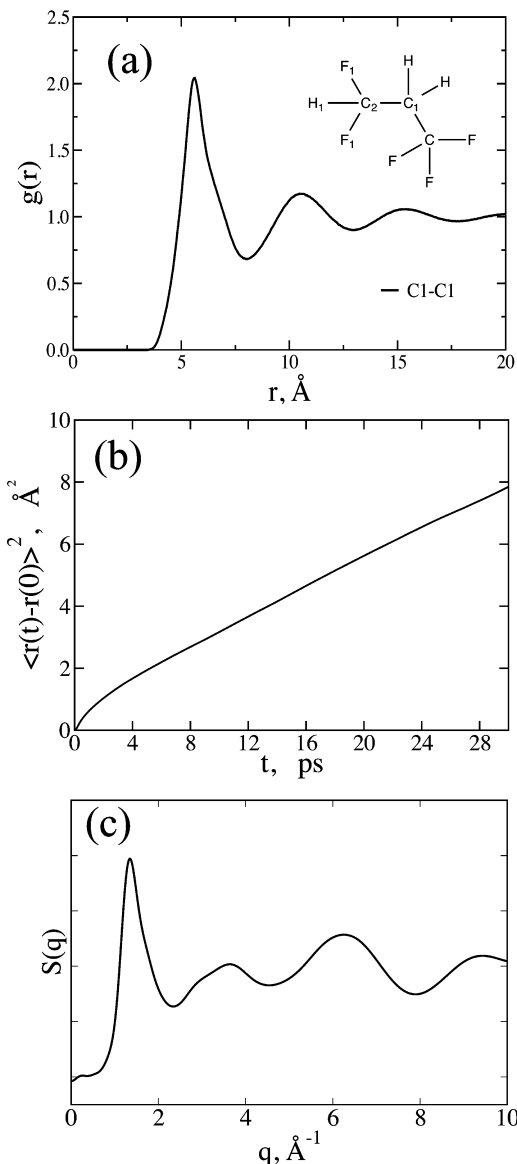


**Figure 3.** (a) Radial distribution function between the central carbon atoms of R-245fa. (b) Mean square displacement for R-245fa. (c) Structure factor of liquid R-245fa at 273 K.

10.5 Å, respectively. The computed coordination number is 12.4. We also computed the mean square displacement for pure liquid R-245fa (see Figure 3b). Using the computed mean

square displacement, we determined the diffusion constant to be  $4.05 \times 10^{-6} \text{ cm}^2/\text{s}$  at 273 K. Also, the computed X-ray structure factor for R-245fa at 273 K is shown in Figure 3c. The first peak is at a  $q$  value of  $1.3 \text{ \AA}^{-1}$ . This peak corresponds to structural correlations at  $4.8 \text{ \AA}$  distance. Features at  $q$  values larger than  $2 \text{ \AA}^{-1}$  are mostly intramolecular in nature. So far, there are no experimental studies reported on the X-ray structure of R-245fa, so a comparison cannot be made.

**B. Adsorption of R-245fa in MIL-101.** In this section, we discuss the adsorption behavior of R-245fa in MIL-101 using experiments as well as GCMC simulations. In Figure 4a, we

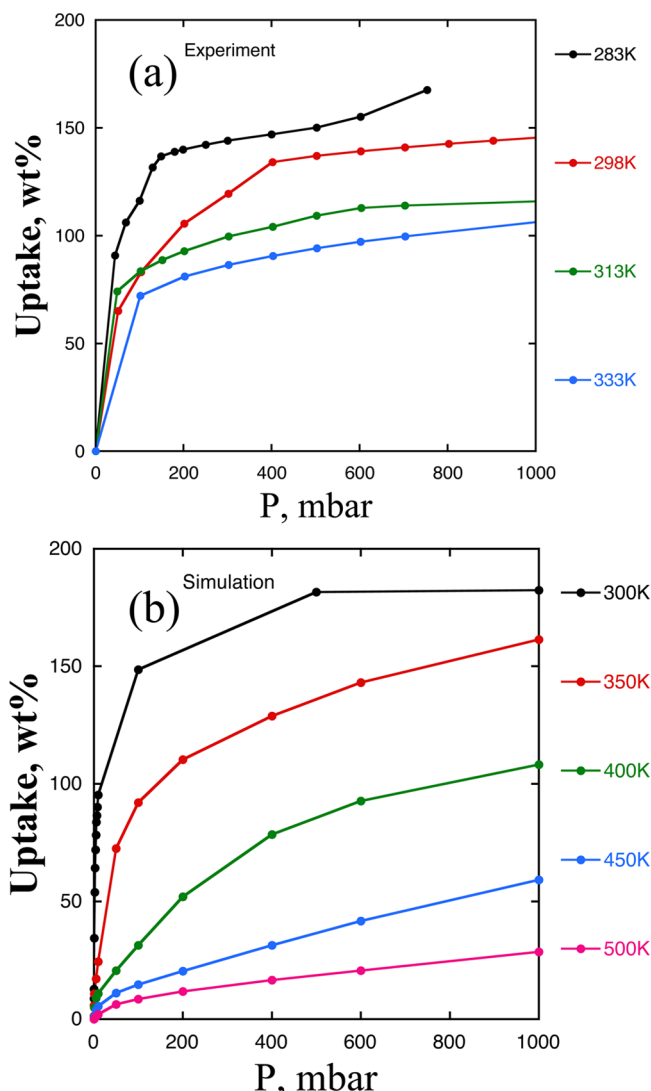


**Figure 4.** (a) Experimental and (b) simulated adsorption isotherms for R-245fa in MIL101 at various temperatures.

show the adsorption isotherms obtained from the experiments as a function of temperature. In Figure 4b, we summarize the adsorption isotherms of R-245fa in MIL-101 at different temperatures ranging from 300 to 500 K. As expected, all the adsorption isotherms increase as the pressure increases and then reach a plateau. The saturated loading at 300 K is 180% by weight. Also, in this plot, it is clear that the gas uptake decreases drastically as temperature increases, because at higher temperatures, molecules have higher velocities and tend to escape, thus leading to low adsorption. Our simulation results overestimated

the experimental data by  $\sim 20\%$  for this system at a similar temperature. This finding indicates that the description of our intermolecular interaction potential models between R-245fa and MIL101 may need further refinement. In Figure 5, we

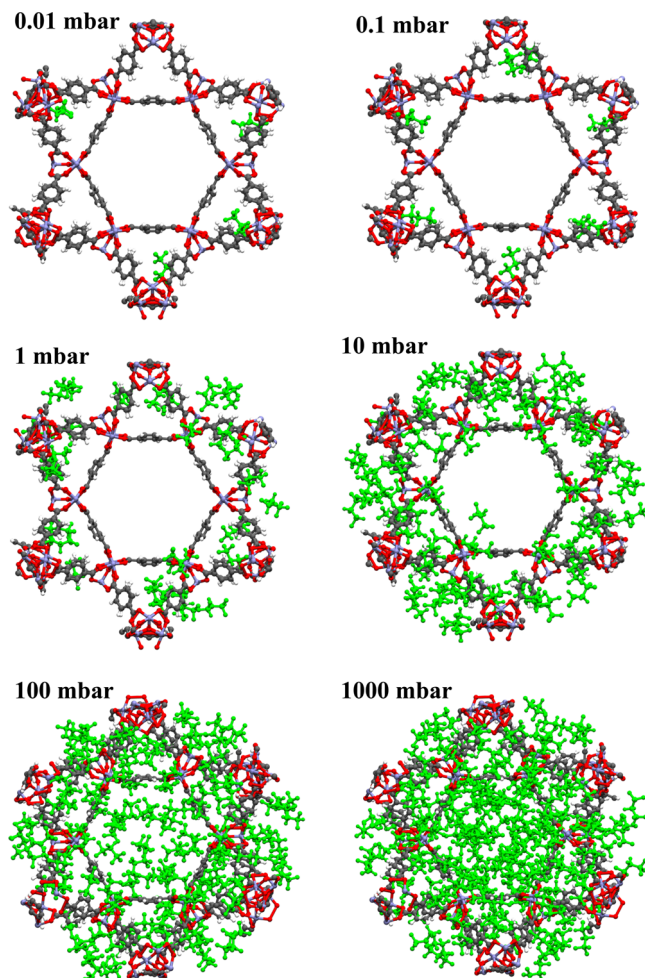


**Figure 5.** GCMC simulation snapshots showing adsorption of R-245fa around the hexagonal window for four different pressures. These snapshots correspond to GCMC simulations at 300 K.

show GCMC simulation snapshots of R-245fa around the hexagonal window at different pressures. At a lower pressure such as 0.01 mbar, the guest molecules are mostly in the tetrahedron cage. As the pressure increases, the molecules begin to appear in the window region as well.

To gain more molecular-level insight on the binding sites, we also performed MD simulations at a loading of 1250 guest molecules. These simulations were carried out in a NVT ensemble with one unit cell of MIL-101 loaded with 1250 R-245fa molecules. The MD run was carried out for 10 ns at 273 K. The computed RDFs are shown in Figures 6a and 6b. In Figure 6a, we show the RDFs between the chromium atoms of the MOF and different carbon atoms of the R-245fa. The Cr-C2 RDF has a very intense first peak at  $\sim 3.5 \text{ \AA}$ , whereas the Cr-C has a negligible peak at  $\sim 3.5 \text{ \AA}$ . The first peak for the Cr-C1 RDF is broader and shifted to the right. This intense peak of Cr-C2 clearly indicates a strong orientation dependence of binding. This behavior could occur because fluorine atoms (F1) on C2 carbon are more partially negative compared to the fluorine atoms (F) on the C carbon atom. In Figure 6b,

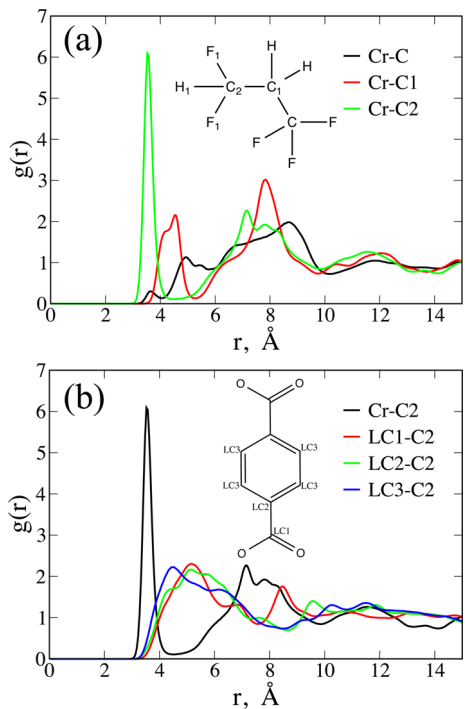


**Figure 6.** (a) RDFs between the different atoms of R-245fa and chromium atoms of MIL-101. (b) RDFs between the C2 carbon of R-245fa and different atoms on MOF.

we show the RDFs between the C2 atom of the R-245fa and different atoms of the MOF (atom are labeled in the inset). The Cr–C2 peak is more intense and occurs further toward the

left compared to the other RDF plots, which clearly indicates the favorable binding to the metal sites compared to linker.

**C. Nanofluid Stability in Water and R-245fa.** In this section, we discuss our studies on the stability of nano-MIL-101-based nanofluids. First, we focused on the solvent structure around the MOF fragments. To this end, we performed two separate MD simulations: one with the MOF fragment solvated in R-245fa, and the other with the MOF fragment solvated in water. The computed RDFs are shown in Figure 7a–d. In Figure 7a, we show the RDF plots between chromium atoms of MOF fragments and the carbon atoms on the R-245fa. Similar to Figure 6a, we observe that the Cr–C2 RDF has a high intense first peak because the fluorine atoms on the C2 carbon atom are more partially negative. In Figure 7b, we show the RDF plots between the chromium atoms and water. The first peak of the Cr–OW RDF occurs at 2.24 Å, and is more intense compared to the Cr–HW RDF because of the strong electrostatic interactions between the Cr atoms of MOF and the oxygen in water. In Figure 7c,d, we show the spatial distribution plots for water and R-245fa around the two types of MOF fragments. We would like to note that the spatial distributions were computed from the two separate simulations, and for the sake of comparison, the spatial densities for water and R-245fa are overlaid in plots. The distribution shown corresponds to the occupancy value of 75 for 5000 frames. The blue color corresponds to the water density, and the green color corresponds to the density of R-245fa. These plots clearly show a high water density around the MOF fragment, which clearly indicates that water has a stronger interaction with the MOF fragment than R-245fa. Also, the higher water density in the tetrahedral cavities can be seen clearly because the smaller water molecule can easily penetrate into the tetrahedral cavity. The significant distribution of R-245fa is found only near the

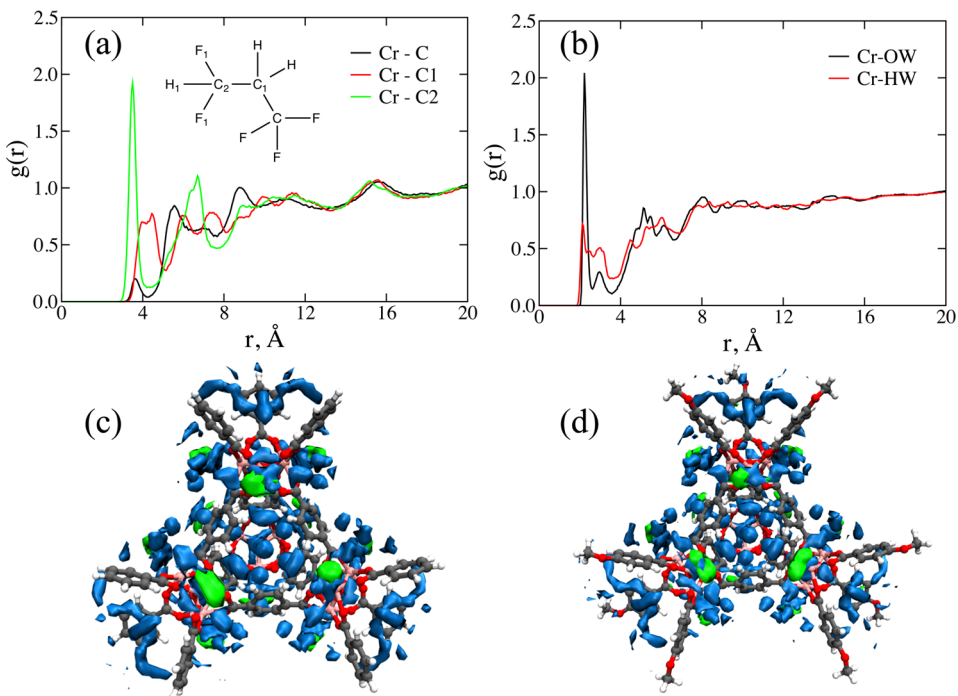


**Figure 7.** (a) Radial distribution function between chromium atoms of MOF fragment and the carbon atoms on the R-245fa. The atoms are labeled in the inset. (b) Radial distribution function between chromium atoms of MOF fragment and water. Spatial distribution of water (blue) and R-245fa (green) round the MOF fragments. (c) MOF fragment with benzoate as the modulator. (d) MOF fragment with 4-methoxy benzoate as the modulator.

chromium sites of the MOF. R-245fa is composed mostly of fluorine atoms, which are partially negative; hence, it interacts favorably only with the positive chromium sites.

In Figure 8a, we show the computed PMF between two MOF fragments with benzoate as modulator (shown in Figure

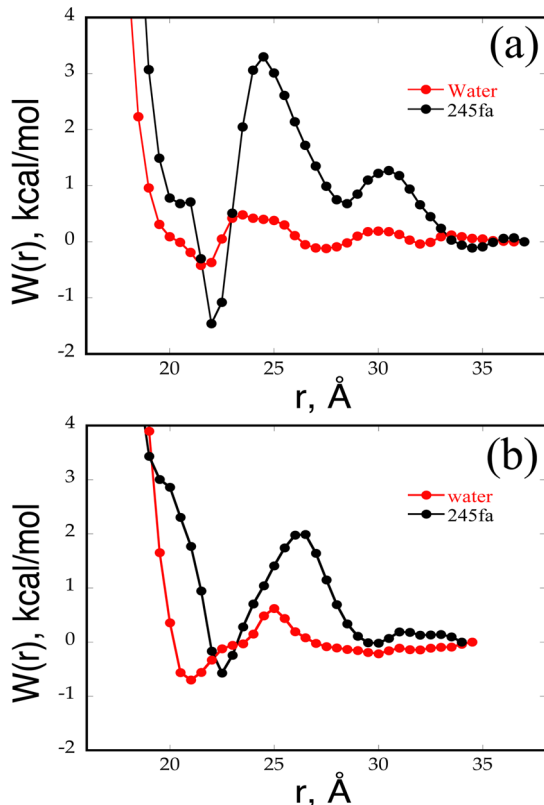


**Figure 8.** (a) Computed PMF for a pair of MOF fragments (shown in Figure 1c) in water and R-245fa. (b) Computed PMF for a pair of MOF fragments (shown in Figure 1d) in water and R-245fa.

1c) in water and R-245fa. Both the PMFs have multiple minima, which indicates that the MOF fragments have solvent-mediated interactions. This behavior is analogous to contact pairs and solvent-separated pairs observed in aqueous salt solutions.<sup>28</sup> The first minimum is at  $\sim 21.5$  Å for water and at  $\sim 22$  Å for R-245fa. The first peak in the PMF plot, also called the barrier, is at  $\sim 23.5$  Å for water and  $\sim 24.5$  Å for R-245fa. This peak is considered as a transition state for the separation of the two MOF fragments; therefore, the higher the barrier height, the greater the amount of energy needed to separate the MOF fragments. The barrier height is 4.8 kcal/mol for R-245fa and 0.9 kcal/mol for water. These values clearly indicate that MOF fragments have strong attractive interactions in R-245fa compared to water. In other words, these MOF fragments are more dispersible in water compared to R-245fa. The degree to which MOF particles disperse depends on MOF–MOF, MOF–solvent, and solvent–solvent interactions. The strong interaction between water and MOF particles as evident from the RDFs and spatial density plots of Figure 7 leads to effective screening of the attractive forces between the MOF fragments. This could be the reason for the better dispersibility of MOF fragments in water.

Figure 8b contains the PMF plots for MOF fragments with 4-methoxybenzoate as the modulator (shown in Figure 1d). The first minimum in water is at  $\sim 21$  Å and in R-245fa at 22 Å.

Both the PMFs in this case have fewer wiggles compared to the previous case for benzoate-containing fragments. The barrier is at 26 Å for R-245fa and at 25 Å for water. Similar to the previous case, the barrier for R-245fa is shifted slightly to the right. The barrier heights are 2.6 kcal/mol for R-245fa and 1.3 kcal/mol for water. Also similar to the previous case, the barrier height for the separation for MOF fragments in R-245fa is greater than that in water. Therefore, even with the methoxy-substituted modulator, the MOF particles tend to disperse better in water than in R-245fa. These results compare well with our experimental observations as illustrated in Figure 2a,b. As discussed earlier, it can be seen in Figure 2a that nano-MOF particles dispersed in water and formed a stable suspension, whereas in Figure 2b; the nano-MOF particles precipitate in R-245fa.

Also, it is interesting to note that the barrier height for the MOF fragments containing methoxybenzoate (Figure 1c) modulators is less than the barrier height for the MOF fragments with benzoate (Figure 1d) modulators in R-245fa. However, we observed a reverse trend for water for which the barrier height is more for the fragments with methoxybenzoate modulators compared to the fragments with benzoate modulators. This indicates that, by incorporating more polar groups on the modulators, the dispersibility MOF fragments increases in R-245fa and decreases in water.

#### IV. CONCLUSIONS

We carried out computational studies to investigate the stability of nanofluids containing MIL-101 MOF nanoparticles. Using GCMC simulations, we studied the adsorption behavior and its temperature dependence for R-245fa in MIL-101. Our simulations indicate that chromium sites are preferential binding sites for adsorption. We computed the PMF to understand the interaction between MOF particles solvated in water and R-245fa. Also, to understand the effect of functionalization of the MOF particles, we studied two sets of MOF particles in both water and in R-245fa. Our computed free energy profiles indicate that, in both the cases, the MOF particles are more attractive in R-245fa compared to water, which implies that nanofluids with these MOF particles will form a more stable suspension in water than in R-245fa. Our studies on the solvent structure around the MOF particles indicate that water has stronger interaction with the MOF surface. For this reason, water effectively screens the interaction between the MOF particles, and therefore, MOF nanoparticles are well dispersed in water compared to R-245fa. Our simulation results compare well with results obtained from experiments. Also, it is interesting to note that the barrier height decreases significantly in R-245fa upon methoxy substitution on the modulators; whereas, in water, the barrier height increases.

#### ASSOCIATED CONTENT

##### S Supporting Information

Force field parameters for R-245fa, GCMC snapshots at 0.01mbar and 0.1mbar, interaction strength between R-245fa and MIL-101 calculated using the isosteric heats of adsorption ( $q_{st}$ ), SEM images of nano-MIL101a in water, illustration of dispersed nano-MIL-101a, and PXRD of nano-MIL-101a and nano-MIL-101b. This material is available free of charge via the Internet at <http://pubs.acs.org>.

## AUTHOR INFORMATION

### Notes

The authors declare no competing financial interest.

## ACKNOWLEDGMENTS

This work was supported by the U.S. Department of Energy (DOE), Office of Science, Office of Basic Energy Sciences, Division of Chemical Sciences, Geosciences, and Biosciences, and by the Office of Energy Efficiency and Renewable Energy, Geothermal Technologies Program. Pacific Northwest National Laboratory is a multiprogram national laboratory operated for DOE by Battelle.

## REFERENCES

- (1) Buongiorno, J.; Venerus, D. The International Nanofluid Property Benchmark Exercise. *Int. J. Heat Fluid Flow* **2010**, *31*, 246–247.
- (2) Yu, W.; France, D. M.; Choi, S. U. S.; Routbort, J. L. *Review and Assessment of Nanofluid Technology for Transportation and other Applications*; Argonne National Laboratory: Argonne, IL, 2007.
- (3) Maxwell, J. C. *A Treatise on Electricity and Magnetism*, 2nd ed.; Clarendon Press Series: Oxford, U.K., 1881.
- (4) Choi, S. U. S.; Zhang, Z. G.; Yu, W.; Lockwood, F. E.; Grulke, E. A. Anomalous Thermal Conductivity Enhancement in Nanotube Suspensions. *Appl. Phys. Lett.* **2001**, *79*, 2252–2254.
- (5) McGrail, B. P.; Thallapally, P. K.; Blanchard, J.; Nune, S. K.; Jenks, J. J.; Dang, L. X. Metal-Organic Heat Carrier Nanofluids. *Nano Energy* **2013**, *2*, 845–855.
- (6) Dang, L. X.; Annappureddy, H. V. R.; Sun, X. Q.; Thallapally, P. K.; McGrail, B. P. Understanding Nanofluid Stability through Molecular Simulation. *Chem. Phys. Lett.* **2012**, *551*, 115–120.
- (7) Furukawa, H.; Cordova, K. E.; O'Keeffe, M.; Yaghi, O. M. The Chemistry and Applications of Metal-Organic Frameworks. *Science* **2013**, *341*, 1230444.
- (8) Latroche, M.; Surble, S.; Serre, C.; Mellot-Draznieks, C.; Llewellyn, P. L.; Lee, J. H.; Chang, J. S.; Jhung, S. H.; Ferey, G. Hydrogen Storage in the Giant-Pore Metal-Organic Frameworks MIL-100 and MIL-101. *Angew. Chem., Int. Ed.* **2006**, *45*, 8227–8231.
- (9) Lee, J.; Farha, O. K.; Roberts, J.; Scheidt, K. A.; Nguyen, S. T.; Hupp, J. T. Metal-Organic Framework Materials as Catalysts. *Chem. Soc. Rev.* **2009**, *38*, 1450–1459.
- (10) Motkuri, R. K.; Liu, J.; Fernandez, C. A.; Nune, S. K.; Thallapally, P. K.; McGrail, B. P. Metal Organic Frameworks - Synthesis and Applications. In *Industrial Catalysis and Separations*; Apple Academic Press: Waretown, NJ, 2014; pp 61–103.
- (11) Motkuri, R. K.; Annappureddy, H. V. R.; Vijaykumar, M.; Schaeff, H. T.; Martin, P. F.; McGrail, B. P.; Dang, L. X.; Krishna, R.; Thallapally, P. K. Fluorocarbon Adsorption in Hierarchical Porous Frameworks. *Nat. Commun.* **2014**, *5*, 4368.
- (12) Nugent, P.; Belmabkhout, Y.; Burd, S. D.; Cairns, A. J.; Luebke, R.; Forrest, K.; Pham, T.; Ma, S. Q.; Space, B.; Wojtas, L.; Eddaoudi, M.; Zaworotko, M. J. Porous Materials with Optimal Adsorption Thermodynamics and Kinetics for CO<sub>2</sub> Separation. *Nature* **2013**, *495*, 80–84.
- (13) Kishan, M. R.; Tian, J.; Thallapally, P. K.; Fernandez, C. A.; Dalgarno, S. J.; Warren, J. E.; McGrail, B. P.; Atwood, J. L. Flexible Metal-Organic Supramolecular Isomers for Gas Separation. *Chem. Commun.* **2010**, *46*, 538–540.
- (14) Annappureddy, H. V. R.; Motkuri, R. K.; Nguyen, P. T. M.; Truong, T. B.; Thallapally, P. K.; McGrail, B. P.; Dang, L. X. Computational Studies of Adsorption in Metal Organic Frameworks and Interaction of Nanoparticles in Condensed Phases. *Mol. Sim.* **2014**, *40*, 571–584.
- (15) Ferey, G.; Mellot-Draznieks, C.; Serre, C.; Millange, F.; Dutour, J.; Surble, S.; Margiolaki, I. A Chromium Terephthalate-Based Solid with Unusually Large Pore Volumes and Surface Area. *Science* **2005**, *309*, 2040–2042.
- (16) Liu, Q.; Ning, L. Q.; Zheng, S. D.; Tao, M. N.; Shi, Y.; He, Y. Adsorption of Carbon Dioxide by MIL-101(Cr): Regeneration Conditions and Influence of Flue Gas Contaminants. *Sci. Rep.* **2013**, DOI: 10.1038/srep02916.
- (17) Case, D. A.; Darden, T. A.; Cheatham III, T. E.; Simmerling, C. L.; Wang, J.; Duke, R. E.; Luo, R.; Merz, K. M.; Pearlman, D. A.; Crowley, M. et al. *Amber* 9; University of California: San Francisco, CA, 2006.
- (18) Gupta, A.; Chempath, S.; Sanborn, M. J.; Clark, L. A.; Snurr, R. Q. Object-Oriented Programming Paradigms for Molecular Modeling. *Mol. Sim.* **2003**, *29*, 29–46.
- (19) Frisch, M. L.; Trucks, G. W.; Schlegel, H. B.; Scuseria, G. E.; Robb, M. A.; Cheeseman, J. R.; Zakrzewski, V. G.; Montgomery, J. A. Jr.; Stratmann, R. E.; Burant, J. C. et al. *Gaussian* 98, revision A.6; Gaussian, Inc.: Pittsburgh, PA, 1998.
- (20) Wang, J. M.; Wolf, R. M.; Caldwell, J. W.; Kollman, P. A.; Case, D. A. Development and Testing of a General Amber Force Field. *J. Comput. Chem.* **2004**, *25*, 1157–1174.
- (21) Wang, J. M.; Wang, W.; Kollman, P. A.; Case, D. A. Automatic Atom Type and Bond Type Perception in Molecular Mechanical Calculations. *J. Mol. Graph. Model.* **2006**, *25*, 247–260.
- (22) Chen, Y. F.; Babarao, R.; Sandler, S. I.; Jiang, J. W. Metal Organic Framework MIL-101 for Adsorption and Effect of Terminal Water Molecules: From Quantum Mechanics to Molecular Simulation. *Langmuir* **2010**, *26*, 8743–8750.
- (23) Berendsen, H. J. C.; Griger, J. R.; Straatsma, T. P. The Missing Term in Effective Pair Potentials. *J. Phys. Chem.* **1987**, *91*, 6269–6271.
- (24) Hansen, J. P.; McDonald, I. P. *Theory of Simple Liquid*; Academic: London, 1986.
- (25) Wolf, D.; Kebbinski, P.; Phillpot, S. R.; Eggebrecht, J. Exact Method for the Simulation of Coulombic Systems by Spherically Truncated, Pairwise 1/R Summation. *J. Chem. Phys.* **1999**, *110*, 8254–8282.
- (26) Essmann, U.; Perera, L.; Berkowitz, M. L.; Darden, T.; Lee, H.; Pedersen, L. G. A Smooth Particle Mesh Ewald Method. *J. Chem. Phys.* **1995**, *103*, 8577–8593.
- (27) Ryckaert, J. P.; Ciccotti, G.; Berendsen, H. J. C. Numerical-Integration of Cartesian Equations of Motion of a System with Constraints Molecular Dynamics of N-Alkanes. *J. Comp. Phys.* **1977**, *23*, 327–341.
- (28) Annappureddy, H. V. R.; Dang, L. X. Molecular Mechanism of Specific Ion Interactions between Alkali Cations and Acetate Anion in Aqueous Solution: A Molecular Dynamics Study. *J. Phys. Chem. B* **2012**, *116*, 7492–7498.